

On the electron temperatures in high-metallicity H II regions

L.S. Pilyugin¹ and L. Mattsson² and J.M. Vílchez³ and B. Cedrés³

¹ *Main Astronomical Observatory of National Academy of Sciences of Ukraine, 27 Zabolotnogo str., 03680 Kiev, Ukraine*

² *Department of Physics and Astronomy, Uppsala University, Uppsala, Sweden*

³ *Instituto de Astrofísica de Andalucía, CSIC, Apdo, 3004, 18080 Granada, Spain*

Accepted 2009 June 3. Received 2009 June 1; in original form 2009 May 12

ABSTRACT

The electron temperatures of high-metallicity ($12 + \log(\text{O}/\text{H}) > 8.2$) H II regions have been studied. The empirical ff relations which express the nebular-to-auroral [O III] line ratio $Q_{3,\text{O}}$ (as well as the nebular-to-auroral [O II] line ratio $Q_{2,\text{O}}$, and the nebular-to-auroral [N II] line ratio $Q_{2,\text{N}}$) in terms of the nebular R_3 and R_2 line fluxes in spectra of high-metallicity H II regions are derived, and the electron temperatures $t_{3,\text{O}}$, $t_{2,\text{O}}$, and $t_{2,\text{N}}$ in a number of extragalactic H II regions are also determined. Furthermore, the $t_2 - t_3$ diagram is discussed. It is found that there is a one-to-one correspondence between t_2 and t_3 electron temperatures for H II regions with a weak nebular R_3 lines ($\log R_3 \lesssim 0.5$). The derived $t_{2,\text{N}} - t_{3,\text{O}}$ relation for these H II regions is similar to commonly used $t_2 - t_3$ relations. The H II regions with a strong nebular R_3 line flux ($\log R_3 \gtrsim 0.5$) do not follow this relation. A discrepancy between $t_{2,\text{N}}$ and $t_{2,\text{O}}$ temperatures is found, being the $t_{2,\text{N}}$ temperatures systematically lower than $t_{2,\text{O}}$ ones. The differences are small at low electron temperatures and increases with increasing electron temperatures up to 10% at $t = 1$. The uncertainties in the atomic data may be the cause of this discrepancy.

Key words: galaxies: abundances – ISM: abundances – H II regions

1 INTRODUCTION

The two-zone model describing the electron temperatures within H II regions is commonly used for oxygen abundance determination (see, e.g., Campbell, Terlevich & Melnick 1986; Garnett 1992). It is typically used when only the electron temperature t_3 is measured and the value of the other temperature t_2 is estimated using a $t_2 - t_3$ relation. Since the form of the $t_2 - t_3$ relation may be disputed (Pilyugin, Vílchez & Thuan 2006; Pilyugin 2007, and references therein) the value of t_2 can be rather uncertain even if accurate measurements of t_3 are available.

The majority of H II regions in spiral galaxies are low excitation objects (Zaritsky, Kennicutt & Huchra 1994, e.g.) and, consequently, the O^+ zone makes a significant (or even dominant) contribution to the total oxygen abundance. This shows that an accurate determination of t_2 is crucial for abundance determinations in H II regions of spiral galaxies. Furthermore, the nitrogen abundances in H II regions are derived from a relation of the form $\text{N}/\text{O} = f(t_2)$. This, again, underlines that accurate determinations of t_2 is very important.

The main objective of the present study is to find the electron temperatures in the zones of singly and doubly

ionised oxygen, and a relation between them. The measured ratio $Q_{2,\text{N}}$ of nebular-to-auroral lines of singly ionised nitrogen is used to determine the electron temperature $t_{2,\text{N}}$ in the low-ionization zone of the H II regions, and the measured ratio $Q_{2,\text{O}}$ of nebular-to-auroral lines of singly ionised oxygen is used to determine the electron temperature $t_{2,\text{O}}$. One may expect that $t_{2,\text{N}}$ and $t_{2,\text{O}}$ are the same, or at least similar. The measured ratio $Q_{3,\text{O}}$ of nebular-to-auroral lines of doubly ionised oxygen is used to determine the electron temperature $t_{3,\text{O}}$ in the high-ionisation zone of the H II regions.

A comparison between different electron temperatures reveals some problems. First of all, the precision of the measurements of the weak auroral lines [O II] $\lambda 7320 + \lambda 7330$, [N II] $\lambda 5755$, and [O III] $\lambda 4363$ is usually low. Secondly, a comparison between different electron temperatures requires a set of H II regions where measurements of the auroral lines [O II] $\lambda 7320 + \lambda 7330$, [N II] $\lambda 5755$, and [O III] $\lambda 4363$ are all available. Such measurements are quite scarce, but that problem may be tackled by constructing the corresponding ff relations. The ff relations allows us to estimate the $Q_{2,\text{N}}$, $Q_{2,\text{O}}$, and $Q_{3,\text{O}}$ values simultaneously (and, consequently,

to determine $t_{2,N}$, $t_{2,O}$, and $t_{3,O}$ electron temperatures) in large samples of H II regions (Pilyugin 2005; Pilyugin 2007).

This paper is organised as follows. The adopted set of the atomic data used to convert the measured line ratios to the electron temperatures is discussed in Section 2. The ff relations for $Q_{3,O}$, $Q_{2,O}$ and $Q_{2,N}$ are derived in Section 3. The relations between different temperatures are examined in Section 4. The results are discussed in Section 5 and Section 6 presents the conclusions.

Throughout this paper, we will be using the following notations for the line fluxes:

$$R = [\text{O III}]\lambda 4363 = I_{[\text{O III}]\lambda 4363}/I_{\text{H}\beta},$$

$$R_2 = [\text{O II}]\lambda 3727 + \lambda 3729 = I_{[\text{O II}]\lambda 3727 + \lambda 3729}/I_{\text{H}\beta},$$

$$R_3 = [\text{O II}]\lambda 4959 + \lambda 5007 = I_{[\text{O II}]\lambda 4959 + \lambda 5007}/I_{\text{H}\beta},$$

$$R_{23} = R_2 + R_3,$$

$$[\text{O II}]\lambda 7325 = [\text{O II}]\lambda 7320 + \lambda 7330 = I_{[\text{O II}]\lambda 7320 + \lambda 7330}/I_{\text{H}\beta},$$

$$[\text{N II}]\lambda 5755 = I_{[\text{N II}]\lambda 5755}/I_{\text{H}\beta},$$

$$N_2 = [\text{N II}]\lambda 6548 + \lambda 6584 = I_{[\text{N II}]\lambda 6548 + \lambda 6584}/I_{\text{H}\beta},$$

$$S_2 = [\text{S II}]\lambda 6717 + \lambda 6731 = I_{[\text{S II}]\lambda 6717 + \lambda 6731}/I_{\text{H}\beta}.$$

With these definitions, the excitation parameter P can be expressed as:

$$P = R_3/(R_2 + R_3),$$

and the temperature indicators $Q_{2,O}$, $Q_{3,O}$ and $Q_{2,N}$ can be expressed as:

$$Q_{2,O} = R_2/[\text{O II}]\lambda 7325,$$

$$Q_{2,N} = N_2/[\text{N II}]\lambda 5755,$$

$$Q_{3,O} = R_3/R.$$

2 DETERMINATION OF ELECTRON TEMPERATURES

To convert the values of the $Q_{3,O}$, $Q_{2,O}$, and $Q_{2,N}$ to the electron temperatures $t_{3,O}$, $t_{2,O}$, and $t_{2,N}$, we have used the five-level-atom solution for ions O^{++} , O^+ , and N^+ together with recent atomic data. The Einstein coefficients for spontaneous transitions A_{jk} for five low-lying levels for all ions above were taken from Froese Fisher & Tachiev (2004). The energy levels were taken from Edlén (1985) for O^{++} , from Wenåker (1990) for O^+ , and from Galavís, Mendoza & Zeippen (1997) for N^+ . The effective cross-sections, or effective collision strengths, for the electron impact Ω_{jk} were taken from Aggarwal & Keenan (1999) for O^{++} , from Pradhan et. al. (2006) for O^+ , and from Hudson & Bell (2005) for N^+ . The effective cross-sections are continuous functions of temperatures, as tabulated by Aggarwal & Keenan (1999); Pradhan et. al. (2006); Hudson & Bell (2005) at a fixed temperatures. The effective cross sections for a given electron temperature are derived from two-order polynomial fits to the data (from the studies cited above) as a function of temperature.

In the low density regime ($n_e < 500 \text{ cm}^{-3}$), the following simple expressions provide good approximations of the numerical results. For the $t_{3,O} - Q_{3,O}$ relation

$$t_{3,O} = \frac{1.46}{\log Q_{3,O} + C_t}, \quad (1)$$

where

$$C_t = -0.88 - 0.17 \log t_{3,O} + 0.030 t_{3,O}, \quad (2)$$

and for $t_{2,O} - Q_{2,O}$,

$$t_{2,O} = \frac{0.96}{\log Q_{2,O} + C_t}, \quad (3)$$

where

$$C_t = -0.86 - 0.38 \log t_{2,O} + 0.053 t_{2,O} + \log(1 + 14.9 x_{2,O}), \quad (4)$$

and

$$x_{2,O} = 10^{-4} n_e t_{2,O}^{-1/2}. \quad (5)$$

Similarly, for the $t_{2,N} - Q_{2,N}$ relation

$$t_{2,N} = \frac{1.12}{\log Q_{2,N} + C_t}, \quad (6)$$

where

$$C_t = -0.89 - 0.19 \log t_{2,N} + 0.032 t_{2,N} + \log(1 + 0.26 x_{2,N}), \quad (7)$$

and

$$x_{2,N} = 10^{-4} n_e t_{2,N}^{-1/2}. \quad (8)$$

These equations can be used instead of computing the electron temperature in low-density H II regions numerically.

3 FF RELATIONS

It has been argued that the excitation parameter P , combined with the measured fluxes of the strong nebular oxygen lines, can be used to estimate the physical conditions in the H II region (Pilyugin 2000, 2001, 2003). One may also say that the electron temperature in an H II region may be estimated using the nebular oxygen line fluxes only, since the excitation parameter P in itself is defined in terms of the nebular oxygen line fluxes, i.e., the diagnostic line ratios can be expressed in terms of just the fluxes of the oxygen nebular lines. It has been found empirically that there exist a relation (the ff relation) between auroral $[\text{O III}]\lambda 4363$ and nebular oxygen line fluxes in spectra of H II regions (Pilyugin 2005; Pilyugin, Thuan & Vílchez 2006). It has been also shown that there exist a relation between $Q_{2,N}$ and nebular oxygen-line fluxes in spectra of H II regions (Pilyugin 2007). Here, relations of this type are derived for $Q_{3,O}$, $Q_{2,O}$ and $Q_{2,N}$.

3.1 A sample of the calibration data

The reliability of the derived ff relations depend on the quality of the calibration data, i.e., on the accuracy of the auroral $[\text{N II}]\lambda 5755$, $[\text{O II}]\lambda 7325$ and $[\text{O III}]\lambda 4363$ line measurements in the H II regions, which are used in deriving the relations. We have compiled a sample of the most reliable spectrophotometric measurements of H II regions from the literature in the following way. First of all, we have only considered recent (published after 2000) observations and line measurements in the spectra of H II regions. Then, we selected the most reliable measurements based on the following criteria. The main requirement is that the uncertainty in the measured electron temperature $t_{3,O}$ (or $t_{2,O}$, or $t_{2,N}$) is less than around 10%. The estimated uncertainties given in the original publications were used. Furthermore, if the measurements of the electron temperatures for two or more ions (e.g. O^{++} and S^{++}) were available for the H II region then the agreement (or disagreement) between these temperatures was used as

an additional criterion: the difference between electron temperatures derived for O^{++} and S^{++} should not be in excess of 1000 K.

We believe that our criteria allow us to pick out the spectra of H II regions with reliable measurements of at least one auroral line ($[N\text{ II}]\lambda 5755$, $[O\text{ II}]\lambda 7325$ and $[O\text{ III}]\lambda 4363$). Our final list consists of 76 spectra of H II regions taken from Guseva, Izotov & Thuan (2000); Luridiana et al. (2002); Vermeij et al. (2002); Kennicutt, Bresolin & Garnett (2003); Lee et al. (2003); Tsamis et al. (2003); Peimbert (2003); Vílchez & Iglesias-Páramo (2003); Bresolin et al. (2004); Izotov & Thuan (2004); Garnett, Kennicutt & Bresolin (2004); Lee & Skillman (2004); Lee, Salzer & Melbourne (2004); Bresolin et al. (2005); Thuan & Izotov (2005); Crockett et al (2006); Bresolin (2007). The measured $[O\text{ II}]\lambda 3727 + \lambda 3729$, $[O\text{ III}]\lambda 4363$, $[O\text{ III}]\lambda 4959 + \lambda 5007$, $[N\text{ II}]\lambda 5755$, $[N\text{ II}]\lambda 6548 + \lambda 6584$, $[S\text{ II}]\lambda 6717 + \lambda 6731$, $[O\text{ II}]\lambda 7320 + \lambda 7330$ line intensities are listed in Table A1 which is available online. In cases where the $I_{[O\text{ III}]\lambda 4959}$ line is not available, the R_3 is obtained from the relation $R_3 = 1.33 \times I_{[O\text{ III}]\lambda 5007} / I_{H\beta}$. Similarly, if the $I_{[N\text{ II}]\lambda 6548}$ line is not available, the N_2 is obtained from the relation $N_2 = 1.33 \times I_{[N\text{ II}]\lambda 6584} / I_{H\beta}$. It should be noted that if the accuracy of any measured auroral line is expected to be low, the line intensity is set to zero in Table A1.

After this investigation has been completed, a new spectrophotometric measurements for H II regions have been published by Bresolin et al. (2009); Esteban et al. (2009). Those data are used to test the reliability of the relations derived in the present paper.

3.2 The ff relation for $Q_{2,N}$

Fig. 1 shows the electron temperature indicator $Q_{2,N}$ as a function of the R_2 line flux (top panel), excitation parameter P (middle panel) and the R_3 line flux (bottom panel) for the sampled spectra of H II regions, where the auroral nitrogen line $[N\text{ II}]\lambda 5755$ is available. It is evident from Fig. 1 that the $Q_{2,N}$ values show a stronger correlation with the R_3 line flux than with the R_2 line flux. H II regions with different values of the excitation parameter are shown in Fig. 2 by different symbols; $0.3 > P > 0.0$ by filled circles, $0.6 > P > 0.3$ by triangles, $0.8 > P > 0.6$ by plus signs, $1.0 > P > 0.8$ by open circles. Fig. 2 shows that the $Q_{2,N}$ values correlate both with the R_3 line flux and the excitation parameter P . It has been found that an expression of the simple form

$$\log Q_{2,N} = a_1 + a_2 P + a_3 \log R_3 \quad (9)$$

reproduces the calibration data quite well.

The coefficients in Eq.(9) are found using our sample of calibration H II regions as described in Pilyugin (2005); Pilyugin & Thuan (2007). We obtain

$$\log Q_{2,N} = 2.04 + 0.66 P - 0.56 \log R_3, \quad \log R_3 < 0.5. \quad (10)$$

The coefficients in Eq.(10) are found using calibration data with relatively weak R_3 lines ($\log R_3 < 0.5$). The calibration data with strong R_3 lines ($\log R_3 \gtrsim 0.5$) do not follow this relation. A gap in the calibration data with $\log R_3$ around 0.5 prevents us to establish a solid value of the limit of the applicability of the derived relation. This (conservative) value was estimated on the base of other diagram (see Section 5). It

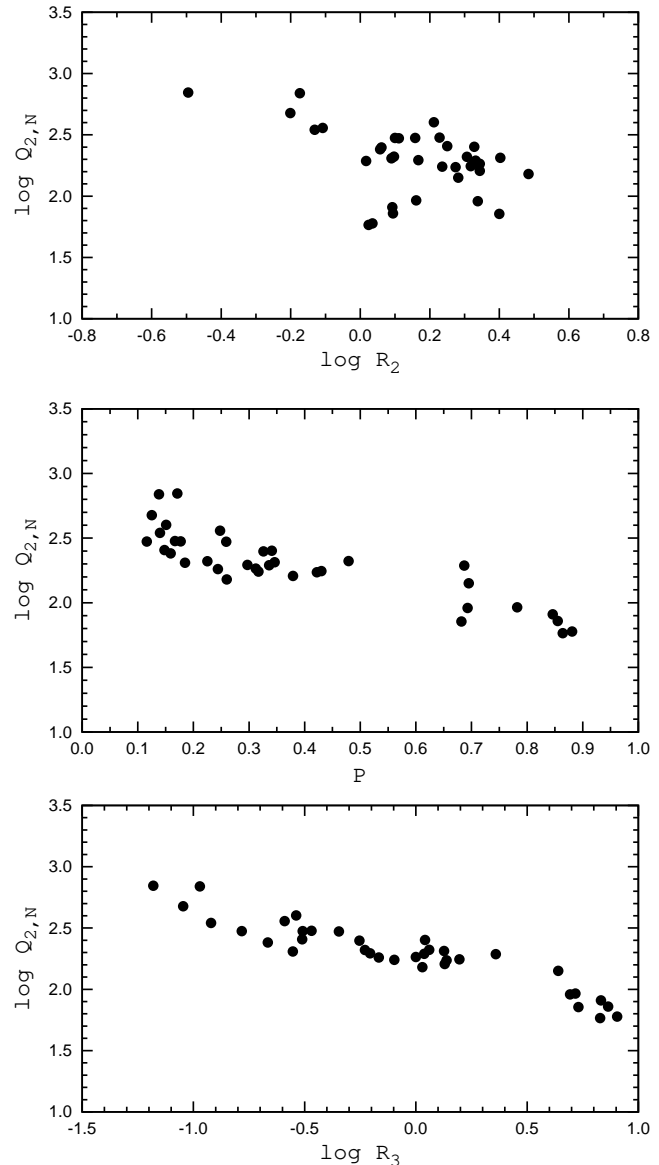


Figure 1. The electron temperature indicator $Q_{2,N}$ as a function of the R_2 line flux (*top panel*), excitation parameter (*middle panel*) and R_3 line flux (*bottom panel*).

is possible that another set of coefficients should be derived for these objects, or a more complex functional form should be used for these objects, or a more complex functional form should be used for these objects in order to reproduce the measurements over the whole interval of R_3 fluxes. This would require more calibration data points (in particular those with strong R_3 lines). The family of $Q_{2,N} = f(R_3, P)$ curves for different values of the excitation parameter is shown in Fig. 2, superimposed on the observational data. The curve with $P = 0.0$ is shown by the solid line, the long-dashed line shows the $P = 0.30$ case, and the short-dashed line shows the $P = 0.6$ case.

Fig. 3 shows the electron temperature $t_{2,N}$ estimated from the derived ff relation and plotted against the measured electron temperature $t_{2,N}$. The filled circles show the H II regions used for calibration. The solid line shows the case of equal values and the dashed lines show $\pm 10\%$ deviations.

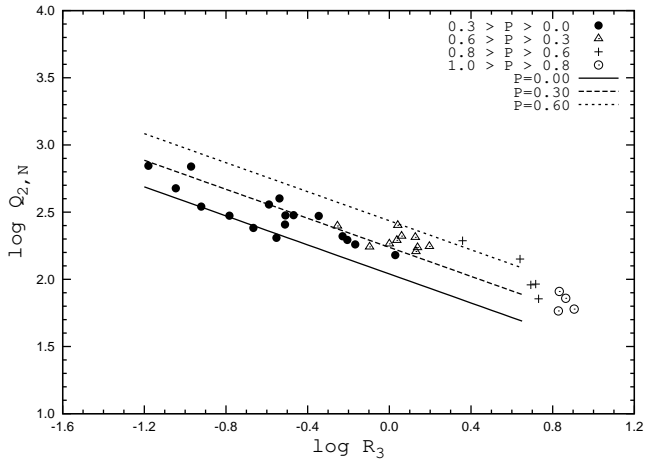


Figure 2. The electron-temperature indicator $Q_{2,N}$ as function of the R_3 line flux. The family of $Q_{2,N} = f(R_3, P)$ curves for different values of the excitation parameter is superimposed on the observational data.

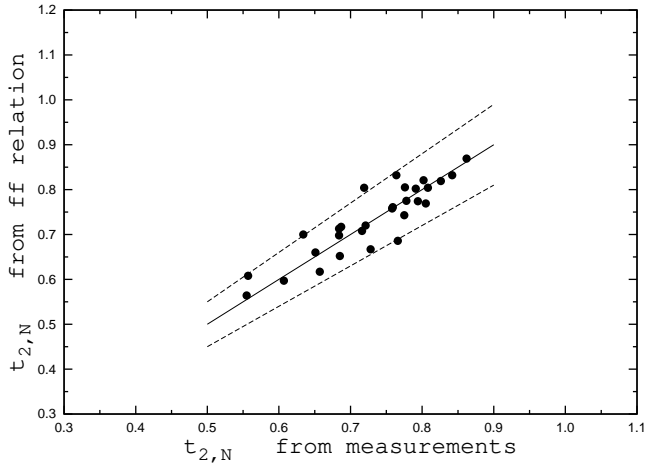


Figure 3. The electron temperature $t_{2,N}$ estimated from the ff relations against the measured electron temperature $t_{2,N}$. The filled circles are the calibration H II regions. The solid line shows the case of equal values and the dashed lines show $\pm 10\%$ deviations.

3.3 The ff relation for $Q_{2,O}$

The sub-sample of H II regions, where the auroral oxygen line $[\text{O II}]\lambda 7325$ is available, has been analysed in a way similar to that of the sub-sample considered in the previous section (see Figs. 4–6). We find the following ff relation for $[\text{O II}]$ lines in the low- R_3 range, ($\log R_3 < 0.5$)

$$\log Q_{2,O} = 1.66 + 0.60 P - 0.46 \log R_3, \quad \log R_3 < 0.5. \quad (11)$$

Again, the calibration data with strong R_3 lines ($\log R_3 \gtrsim 0.5$) do not follow this relation.

3.4 The ff relation for $Q_{3,O}$

An analysis of the sub-sample of H II regions, where the auroral oxygen line $[\text{O III}]\lambda 4363$ is available (see Figs. 7–9) results in the following ff relation for $[\text{O III}]$ lines

$$\log Q_{3,O} = 2.53 + 1.08 P - 1.42 \log R_3. \quad (12)$$

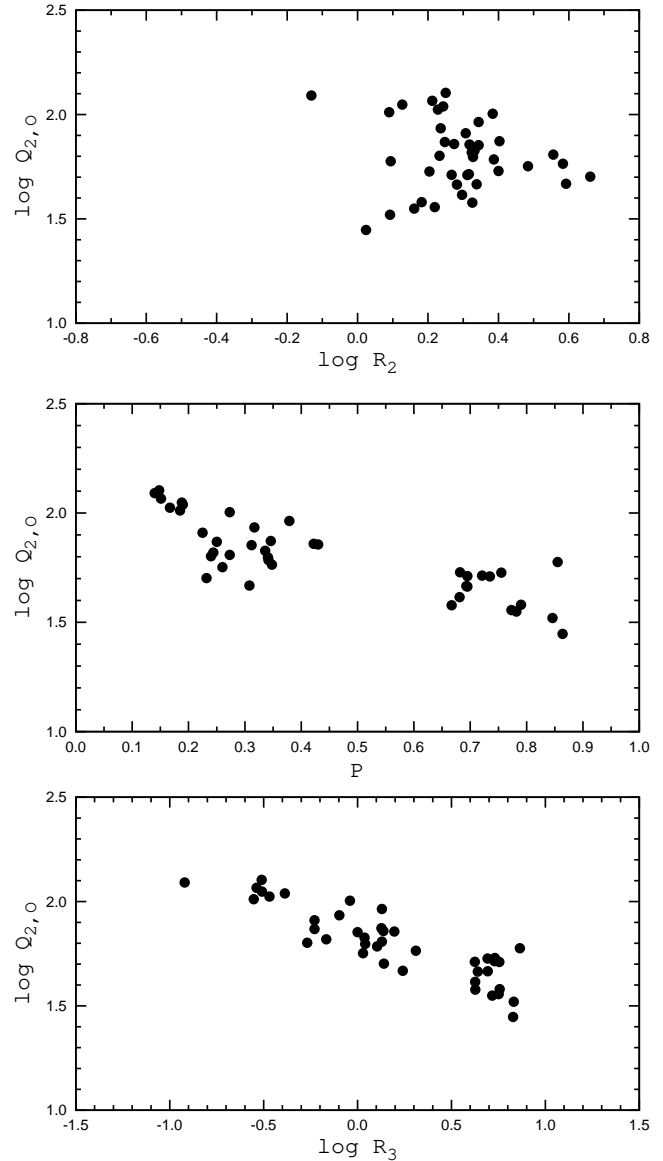


Figure 4. The electron temperature indicator $Q_{2,O}$ as a function of flux the R_2 line flux (*top panel*), excitation parameter (*middle panel*) and R_3 line flux (*bottom panel*).

In this case, the calibration data follow the derived relation over the whole range of R_3 values.

4 RELATIONS BETWEEN ELECTRON TEMPERATURES

4.1 Comparison between $t_{2,N}$ and $t_{2,O}$ temperatures

Fig. 10 shows the $t_{2,N} - t_{2,O}$ diagram. The values of $t_{2,N}$ and $t_{2,O}$ for our sample of extragalactic H II regions with $\log R_3 < 0.5$, estimated using the ff relations, are shown by filled circles (the ff-based temperatures are used because measurements of both $t_{2,N}$ and $t_{2,O}$ temperatures are not available). The dashed line shows the case of equal values. It is evident from Fig. 10 that the $t_{2,N}$ temperatures are systematically lower than $t_{2,O}$ temperatures. At low electron

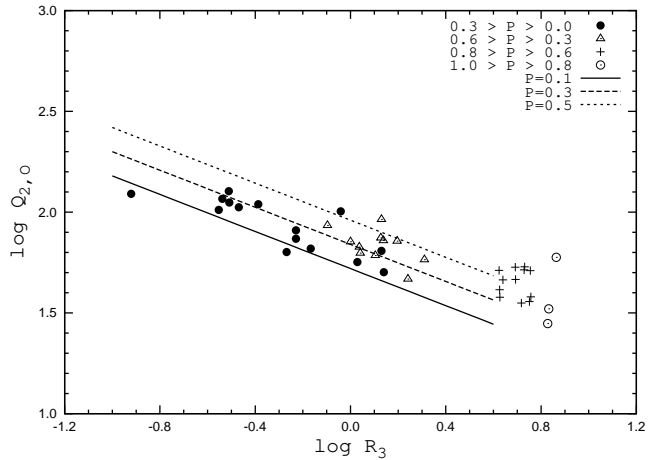


Figure 5. The electron temperature indicator $Q_{2,O}$ against the R_3 line flux. The family of $Q_{2,N} = f(R_3, P)$ curves for different values of the excitation parameter is superimposed on the observational data.

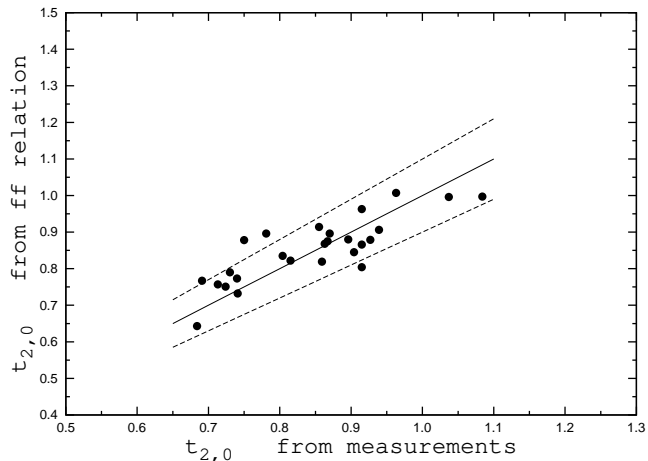


Figure 6. The electron temperature $t_{2,O}$ estimated from the ff relations against the measured electron temperature $t_{2,O}$. The filled circles show the calibration H II regions. The solid line shows the case of equal values and the dashed lines show $\pm 10\%$ deviations.

temperatures the discrepancy is small, but it increases with increasing electron temperature. The difference is around 10% at $t_2 = 1.0$. We find four possible causes for this discrepancy:

(1) The conversion of the strong line fluxes into the temperature indicators $Q_{2,N}$ and $Q_{2,O}$ involve systematic errors, i.e., the ff relation for [N II] lines or/and the ff relation for [O II] lines is/are too crude and involves a systematic error. If this is the case, low precision of the line measurements in the spectra of the calibration H II regions can be the cause of the discrepancy between $t_{2,N}$ and $t_{2,O}$.

(2) The conversion of the temperature indicators $Q_{2,N}$ or/and $Q_{2,O}$ to the electron temperatures $t_{2,N}$ or/and to $t_{2,O}$ involves systematic errors. If this is the case, low precision of the atomic data can be the cause of the the discrepancy between $t_{2,N}$ and $t_{2,O}$.

(3) The value $Q_{2,O}$ and/or $Q_{2,N}$ is/are bad indicators of the

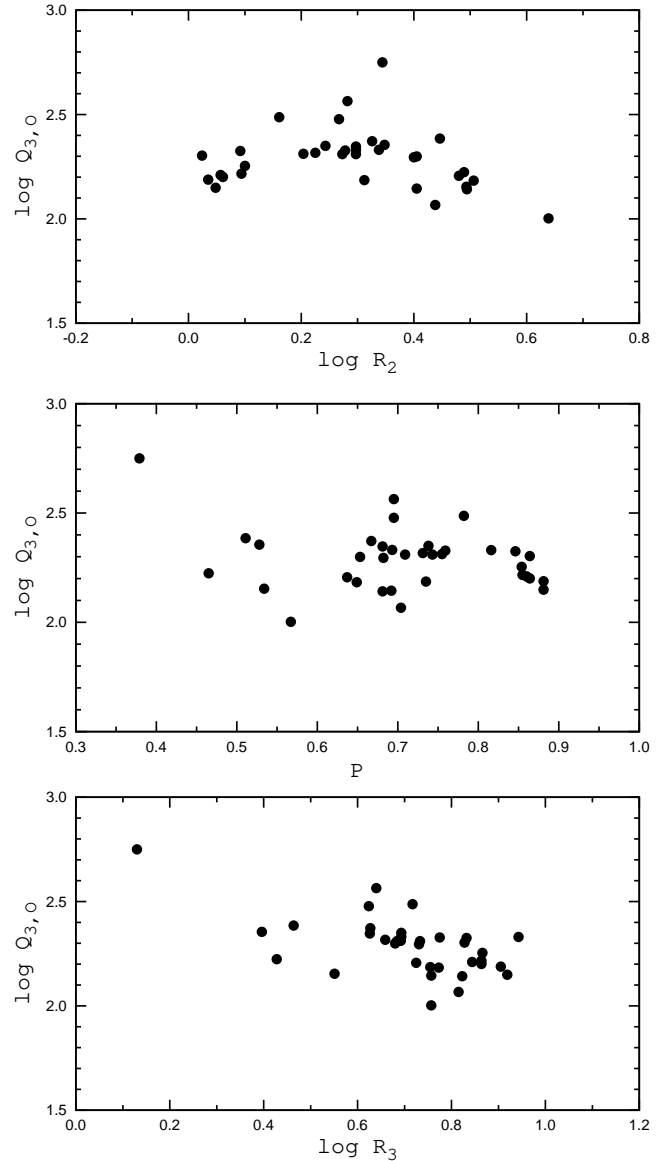


Figure 7. The electron temperature indicator $Q_{3,O}$ as a function of the R_2 line flux (*top panel*), excitation parameter (*middle panel*) and R_3 line flux (*bottom panel*).

electron temperatures and do not reflect the true electron temperature in an H II region.

(4) The the [N II] lines are sometimes blended with the H α lines. In such cases it is possible that the electron temperatures $t_{2,N}$ are affected by the errors occurring when disentangling these two lines. It is quite likely that this is mostly a problem for objects where emission lines are strong, but it is difficult to quantify the effects. Hence, we here only mention this possibility and do not analyse it in any further detail.

We have also considered the effects of absorption from an underlying stellar population. But since absorption effects are pronounced mostly in the Balmer lines, the impact on, e.g., R_2 and R_3 is negligible and cannot be the cause of the discrepancy described above.

Uncertainties in the electron temperatures $t_{3,O}$, $t_{2,O}$ and $t_{2,N}$ caused by uncertainties in the atomic data have been

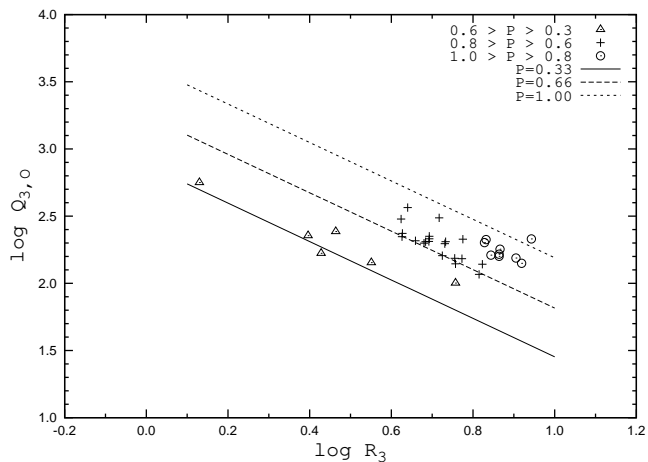


Figure 8. The electron temperature indicator $Q_{3,O}$ against flux in the line R_3 . The family of $Q_{2,N} = f(R_3, P)$ curves for different values of the excitation parameter is superimposed on the observational data.

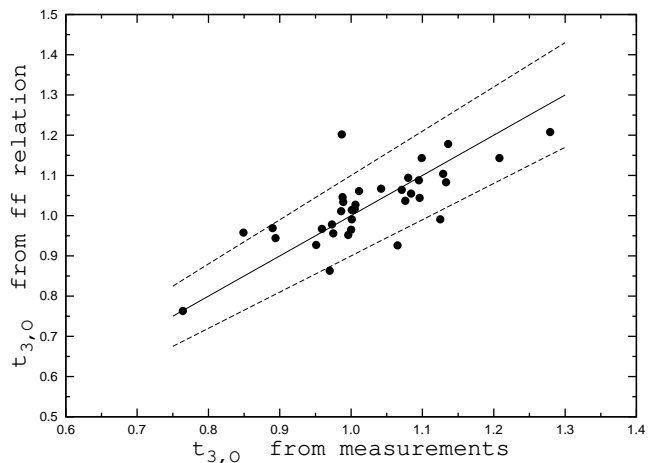


Figure 9. The electron temperature $t_{3,O}$ estimated from the ff relations against the measured electron temperature $t_{3,O}$. The filled circles show the calibration H II regions. The solid line shows the case of equal values and the dotted lines show $\pm 10\%$ deviations.

considered by Pilyugin (2009). Following that work, we like to point out a few critical issues, regarding such uncertainties. To convert the temperature indicator $Q_{2,N}$ into the electron temperature $t_{2,N}$, we have used the five-level-atom solution for N^+ with the Einstein coefficients for spontaneous transitions A_{jk} obtained by Froese Fisher & Tachiev (2004) and the effective cross-sections for electron impact Ω_{jk} from Hudson & Bell (2005). It is expected that the best present effective collision strengths between the low-lying states have a typical uncertainty of around 10% (Hudson & Bell 2004; Tayal 2007). The general accuracy of the present probabilities is expected to be within 10% (Galavis, Mendoza & Zeippen 1997).

The uncertainty in $t_{2,N}$, caused by the uncertainty in the atomic data, can be estimated in the following way. The values of A_{jk} from Froese Fisher & Tachiev (2004) and Ω_{jk} from Hudson & Bell (2005) have been considered as “standard” values. We then introduce a random relative error

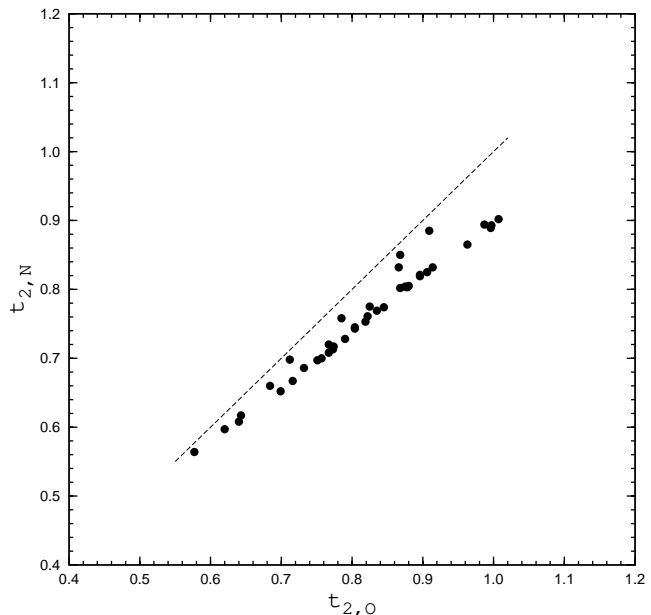


Figure 10. Electron temperature $t_{2,N}$ against electron temperature $t_{2,O}$. The filled circles show $t_{2,N}$ and $t_{2,O}$ in our samples of extragalactic H II regions with $\log R_3 < 0.5$ estimated using the ff relations. The dashed line shows the case of equal values.

from -15% to $+15\%$ to every value of A_{jk} and Ω_{jk} . The electron temperature derived from the five-level-atom solution with a random-error component added to the atomic data will be referred to as $t_{2,N}^*$. The $t_{2,N}^*$ values for a set of $Q_{2,N}$ values were computed with 500 different random errors added to the atomic data. The relative error in the $t_{2,N}$ temperature $\delta t_{2,N} = 1 - t_{2,N}^*/t_{2,N}$ caused by the uncertainties in the atomic data, increases with increasing of electron temperature. The top panel of Fig. 11 shows $\delta t_{2,N}$ at $t = 1$ versus the mean of the absolute values of the relative random error component in Ω_{jk} . The value of $\delta t_{2,N}$ is mainly governed by the uncertainties in the effective collision strengths for transitions from level 1 to levels 4 and 5. When the errors in Ω_{14} and Ω_{15} are large (and have opposite signs), the value of $\delta t_{2,N}$ is large even if the mean of the absolute values of the random error component in Ω_{jk} are small due to small errors in other Ω_{jk} . On the other hand, when the errors in Ω_{14} and Ω_{15} are small then the value of $\delta t_{2,N}$ is small, even if the mean of the absolute values of the random error component in Ω_{jk} are large due to large errors in other Ω_{jk} .

To convert the temperature indicator $Q_{2,O}$ into the electron temperature value $t_{2,O}$, we have used the five-level-atom solution for O^+ with the Einstein coefficients for spontaneous transitions A_{jk} obtained by Froese Fisher & Tachiev (2004) and the effective cross sections for electron impact Ω_{jk} from Pradhan et. al. (2006). Again, the $t_{2,O}^*$ values for a set of $Q_{2,O}$ values were computed with 500 different random errors (from -15% to $+15\%$) added to every value of A_{jk} and Ω_{jk} . The bottom panel of Fig. 11 shows $\delta t_{2,O}$ at $t = 1$ versus the mean of the absolute values of the random error component in Ω_{jk} . The Fig. 11 shows that the value of the error in the electron temperatures $t_{2,O}$ and $t_{2,O}$ caused by uncertainties in the atomic data is comparable with the obtained discrepancy between $t_{2,N}$ and $t_{2,O}$.

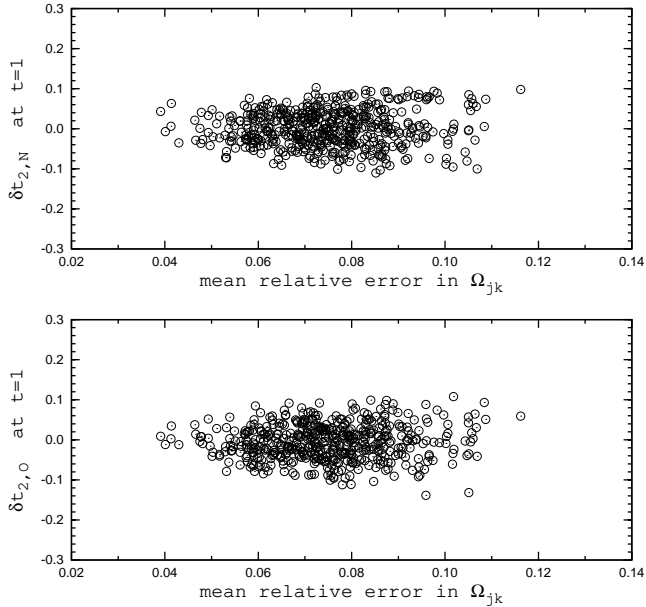


Figure 11. *Upper panel:* the relative difference (at $t = 1$) between the electron temperature $t_{2,N}^*$ derived with a random error component added to the effective cross-sections for electron impact Ω_{jk} and the electron temperature $t_{2,N}$ derived with “standard” atomic data as a function of the average of the absolute values of the relative random error components. *Lower panel:* same as upper panel, but for the electron temperature $t_{2,O}$.

We find that the errors in the electron temperatures $t_{2,N}$ and/or $t_{2,O}$ caused by uncertainties in the atomic data can explain the discrepancy between the electron temperatures $t_{2,N}$ and $t_{2,O}$ that we obtain. However, it should be noted that the errors caused by uncertainties in the ff relation for [O II] lines and/or the ff relation for [N II] lines can also make a contribution to the discrepancy between $t_{2,N}$ and $t_{2,O}$. More high-precision measurements of nitrogen and oxygen auroral lines are needed in order to find better ff relations and to elucidate the origin of the discrepancy between $t_{2,N}$ and $t_{2,O}$.

4.2 The relation between electron temperature in low- and high-ionisation zones

Fig. 12 shows the $t_{2,N} - t_{3,O}$ diagram for H II regions with $\log R_3 < 0.5$. The ff-based $t_{2,N}$ and $t_{3,O}$ temperatures in H II regions are used. The relation between electron temperature in low- and high-ionisation zones has been established on the basis of objects with weak R_3 line fluxes $\log R_3 < 0.5$. The linear relation

$$t_{2,N} = 0.314 + 0.672 t_{3,O}. \quad (13)$$

has been obtained by least-squares fitting. The coefficients in Eq.(13) were derived from the data for H II regions with weak R_3 line fluxes using an iterative fitting routine. Data points with large deviations were excluded in the fit. The resultant $t_{2,N} - t_{3,O}$ relation is shown by the solid line in Fig. 12. There is a trace of non-linearity in the $t_{2,N} - t_{3,O}$ diagram. The origin of this “bending” (if real) can be twofold: It can be artificial and caused by the fact that the particular form of the analytical expression adopted for the ff relation

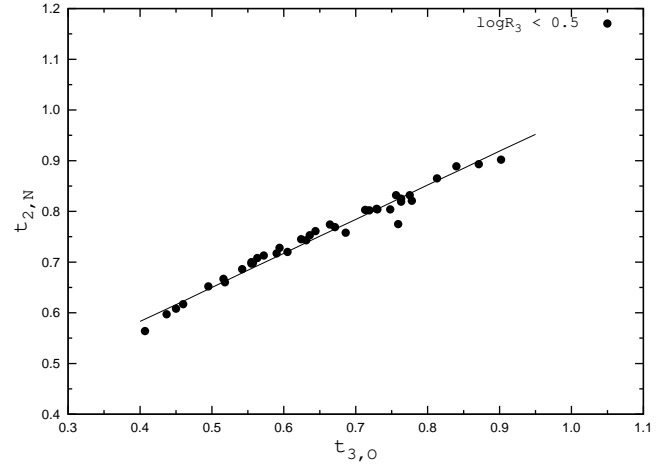


Figure 12. The $t_{2,N} - t_{3,O}$ diagram for H II regions with weak R_3 line fluxes ($\log R_3 < 0.5$). The ff-based $t_{2,N}$ and $t_{3,O}$ temperatures are used. The solid line shows the derived $t_{2,N} - t_{3,O}$ relation.

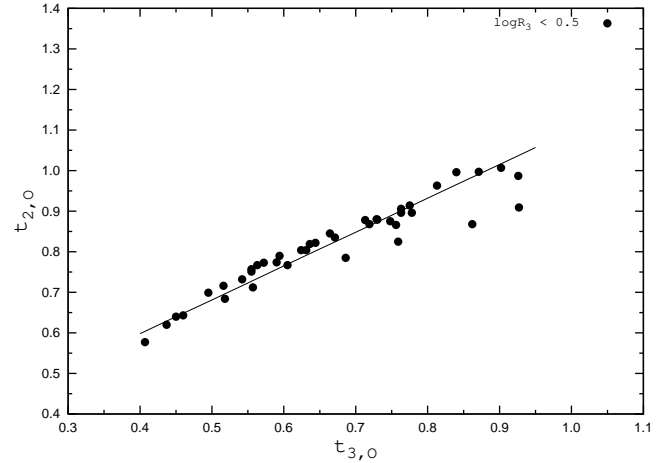


Figure 13. The same as Fig. 12 but for $t_{2,O} - t_{3,O}$ relation.

for [O III] lines and/or the ff relation for [N II]. We have chosen a simple form, but perhaps a more complex expression may give a better fit to the ff relation(s). It may also be that the linear expression adopted here for the $t_{2,N} - t_{3,O}$ relation is inappropriate. It is possible that the expression suggested by Pagel et al. (1992) is more realistic. If so, the relations derived here may be considered as the first-order approximation. More high-precision measurements of nitrogen and oxygen auroral lines are needed to find better relations and to elucidate the origin of the possible non-linearity.

The $t_{2,O} - t_{3,O}$ diagram (Fig. 13) has been examined in a similar way, and we thus obtain the expression

$$t_{2,O} = 0.264 + 0.835 t_{3,O}. \quad (14)$$

This $t_{2,O} - t_{3,O}$ relation is shown by the solid line in Fig. 13. The general properties of the $t_{2,O} - t_{3,O}$ diagram and the $t_{2,N} - t_{3,O}$ diagram are similar. The scatter in the $t_{2,N} - t_{3,O}$ diagram (Fig. 12) is smaller than that in the $t_{2,O} - t_{3,O}$ diagram (Fig. 13). This may suggest that the $t_{2,N}$ temperature is more reliable than the $t_{2,O}$ temperature.

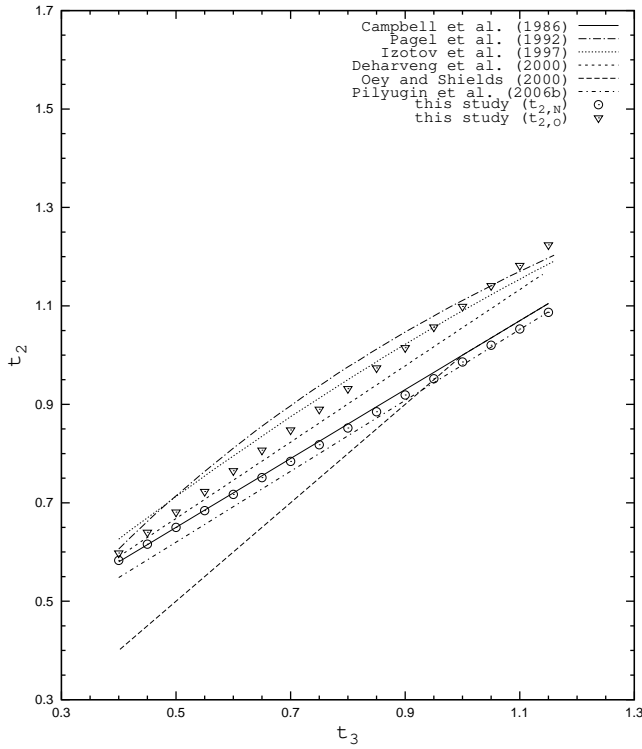


Figure 14. Comparison of the $t_2 - t_3$ relation derived here with those derived by other authors. The different lines are $t_2 - t_3$ relations derived by these authors. Our $t_{2,N} - t_{3,O}$ relation is shown by the circles, and our $t_{2,O} - t_{3,O}$ relation is shown by the triangles.

5 DISCUSSION

Since the electron temperature $t_{2,N}$ seem to be more reliable than $t_{2,O}$, the $t_{2,N} - t_{3,O}$ diagram needs some further discussion.

5.1 The comparison with previous $t_2 - t_3$ relations

We compared the $t_{2,N} - t_{3,O}$ and $t_{2,O} - t_{3,O}$ relations derived here with those obtained by other authors. Since our $t_2 - t_3$ relations are derived for cool, high-metallicity H II regions, the high-temperature and low-metallicity part of the relation is not considered here. The different lines in Fig. 14 are the $t_2 - t_3$ relations by Campbell, Terlevich & Melnick (1986); Pagel et al. (1992); Izotov, Thuan & Lipovetsky (1997); Deharveng et al. (2000); Oey & Shields (2000); Pilyugin, Vílchez & Thuan (2006). Our $t_{2,N} - t_{3,O}$ and $t_{2,O} - t_{3,O}$ relations are shown by the open circles and the open triangles, respectively. Examination of Fig. 14 shows that our $t_{2,N} - t_{3,O}$ relation is very similar to the widely used $t_2 - t_3$ relation after Campbell, Terlevich & Melnick (1986) (see also Garnett (1992)).

Just recently Esteban et al. (2009) derived a $t_{2,N} - t_{3,O}$ relation, which is very close to the one we have obtained here.

5.2 Abundances in spiral galaxy NGC 300

New spectrophotometric observations of H II regions in the spiral galaxy NGC 300 have recently been published by

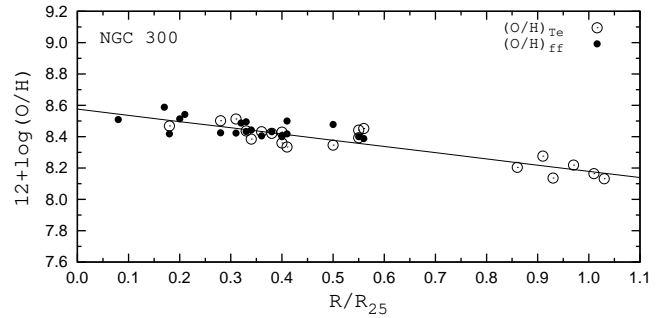


Figure 15. The radial distribution of oxygen abundance in the disk of spiral galaxy NGC 300 traced by H II regions. The open circles are T_e -based abundances, the line is the best fit to those data. The filled circles are ff-based abundances. The galactocentric distance is expressed in terms of the isophotal radius R_{25} .

Bresolin et al. (2009). They have measured the auroral lines, and derived the radial oxygen abundance gradient in the disc of NGC 300 based on “direct” (T_e -based) oxygen abundances. This provides an additional possibility to test the relations we have derived in the present paper.

T_e -based oxygen abundances in H II regions, where the auroral oxygen line $[\text{O III}]\lambda 4363$ is available, are shown in Fig. 15 by the open circles. The line is the linear best fit to those data. We have estimated the t_3 temperature from the ff relation, Eq.(12), and then the t_2 temperature from the $t_2 - t_3$ relation, Eq.(13). Fig. 15 also shows that at the galactocentric distances larger than $\sim 0.7R_{25}$, the oxygen abundance is lower than $12 + \log(\text{O}/\text{H}) = 8.2$ (the R_{25} is the isophotal radius). Therefore, the derived ff relation, Eq. (12), is applicable only to the H II regions with galactocentric distances less than $\sim 0.7R_{25}$. The derived $(\text{O}/\text{H})_{\text{ff}}$ abundances for 20 out of 21 H II regions are shown in Fig. 15 by the filled circles (the H II region # 12 shows a very large deviation and was rejected). The $(\text{O}/\text{H})_{\text{ff}}$ abundances follow well the radial gradient traced by the $(\text{O}/\text{H})_{T_e}$ abundances. This confirms that the relations derived here, result in realistic oxygen abundances.

5.3 Deviations from the $t_2 - t_3$ relation

We have found that the calibration data with strong R_3 lines ($\log R_3 \gtrsim 0.5$) do not follow the ff relation for $Q_{2,N}$. Here, the deviations from the $t_{2,N} - t_{3,O}$ relation are examined. We define the deviation of $t_{2,N}$ from the $t_{2,N} - t_{3,O}$ relation as the difference $\Delta t_{2,N}$ between the measured electron temperature $t_{2,N}$ and electron temperature $t_{2,N}^r$ obtained from the $t_{2,N} - t_{3,O}$ relation and the electron temperature $t_{3,O}$. Fig. 16 shows the deviations $\Delta t_{2,N} = t_{2,N} - t_{2,N}^r$ as a function of R_3 line flux (top panel), excitation parameter P (middle panel) and the electron temperature $t_{3,O}$ (bottom panel). Fig. 12 shows that the H II regions with strong R_3 line fluxes show large deviations from the $t_{2,N} - t_{3,O}$ relation traced by the H II regions with weak R_3 line fluxes.

High-precision spectroscopy, including the auroral line $[\text{N II}]\lambda 5755$, for a number of galactic H II regions can be found in the literature (Esteban et al. 1999a,b, 2004; Baldwin et al. 2000; Tsamis et al. 2003; García-Rojas et al. 2004, 2005, 2006, 2007). These spectroscopic measurements cannot be used to construct the ff re-

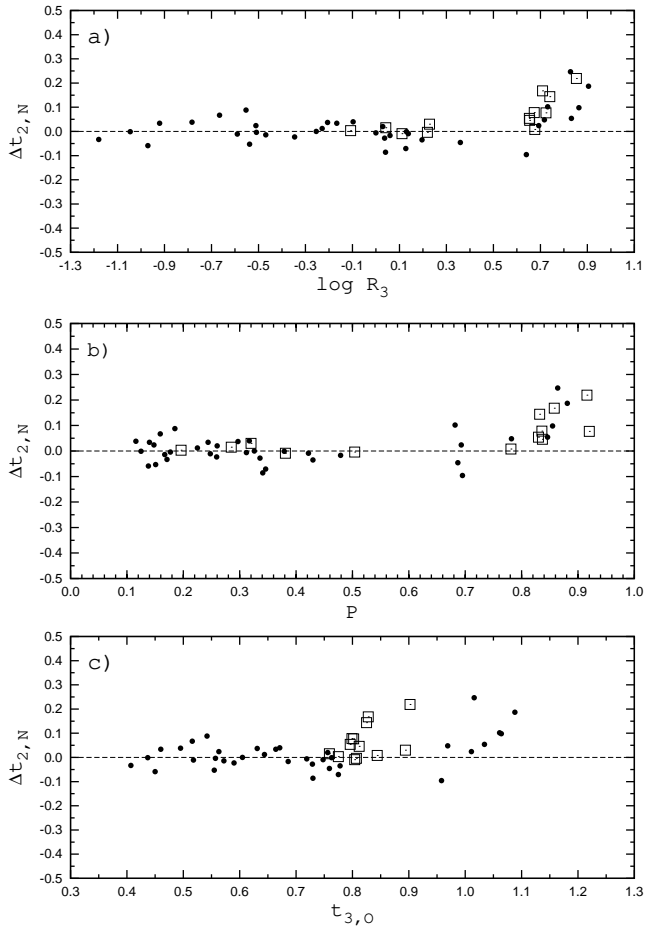


Figure 16. Deviations of $t_{2,N}$ from the $t_{2,N}-t_{3,O}$ relation as a function of R_3 line flux (*top panel*), excitation parameter (*middle panel*) and electron temperature $t_{3,O}$ (*bottom panel*). The filled circles show the deviations estimated using the measured $t_{2,N}$ and ff-based $t_{3,O}$ temperatures in H II regions from our sample. The open squares show the deviations obtained using the measured $t_{3,O}$ and $t_{2,N}$ temperatures in galactic H II regions.

lations since only a small part of the galactic H II regions are measured and, therefore, the obtained excitation-parameter value is not representative for the whole nebula. However, they provide a remarkable possibility to test the derived $t_{2,N} - t_{2,O}$ relation. The open squares in Fig. 16 show the deviations $\Delta t_{2,N}$ of galactic H II regions. The measured $t_{3,O}$ and $t_{2,N}$ temperatures in galactic H II regions are used. Inspection of Fig. 16 shows that the general behaviour of the deviations in the case of galactic H II regions is quite similar to that of extragalactic H II regions. The galactic H II regions with weak R_3 line fluxes follow the derived the $t_{2,N}-t_{3,O}$ relation (the deviations $\Delta t_{2,N}$ are small) and significant deviations occur in the case of galactic H II regions with strong R_3 line fluxes. Thus, the consideration of galactic H II regions confirms the results derived based on extragalactic H II regions.

Fig. 12 shows that there is a one-to-one correspondence between $t_{2,N}$ and $t_{3,O}$ within the uncertainties for H II regions with weak R_3 lines. The H II regions with strong R_3 line fluxes do not follow the $t_{2,N}-t_{3,O}$ relation obtained from the H II regions with weak R_3 line fluxes, and the deviations

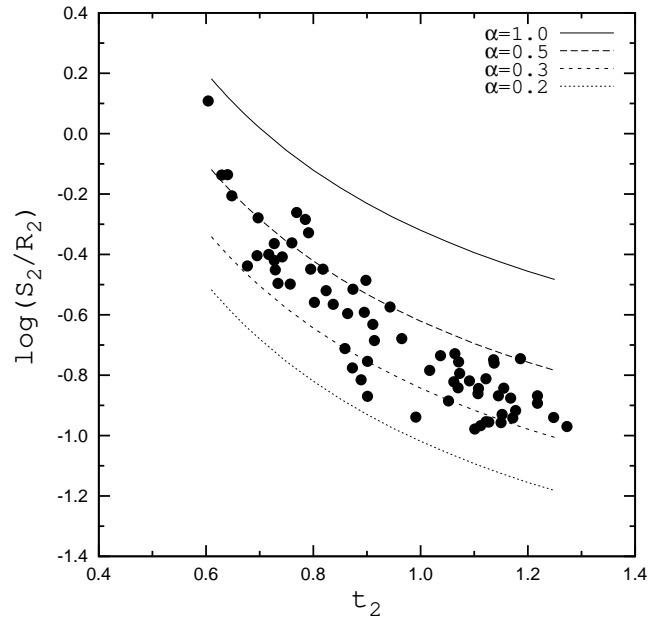


Figure 17. The S_2/R_2 line ratio as a function of electron temperature t_2 . Family of theoretical curves for different values of the parameter α (which is the size ratio of S^+ and O^+ zones) superimposed on the observational data.

$\Delta t_{2,N}$ do not depend on the electron temperature $t_{3,O}$. As a result, the one-to-one correspondence between electron temperatures $t_{2,N}$ and $t_{3,O}$ disappears if a sample contains H II regions with both weak and strong R_3 line fluxes.

5.4 A possible origin of the deviations from the $t_2 - t_3$ relation

One may assume that the S/O abundance ratio is constant in all the H II regions since the sulfur and oxygen are thought to be produced by the same massive stars. It is commonly accepted that the [O II] and [S II] lines are formed at similar temperatures. The energy of the level that gives rise to the R_2 line (the [O II] $\lambda 3727, 3729$ doublet) is higher than the energy of the level giving rise to the S_2 line (the [S II] $\lambda 6717, 6731$ doublet). Thus, the line-emissivity ratio $j(S_2)/j(R_2)$ is temperature sensitive, i.e., the ratio increases with decreasing electron temperature. Furthermore, the S^+ -zone does not coincide with the O^+ -zone. Hence, the S_2/R_2 line ratio depends on two parameters; the electron temperature t_2 and the size ratio of S^+ and O^+ zones α . An analysis of the variation of the S_2/O_2 ratios in H II regions can help to illuminate the reason for the irregularity of high- R_3 H II regions.

Fig. 17 shows the measured S_2/R_2 ratio as a function of electron temperature t_2 (the values $t_{2,O}^r$ are used) for H II regions from our sample together with a family of theoretical curves computed for different values of α

$$\frac{S_2}{R_2} = \alpha \frac{S}{O} \frac{j(S_2)}{j(R_2)}. \quad (15)$$

The solar S/O abundance ratio was used in the computations, i.e., $\log(S/O) = -1.50$ (Lodders 2003). The line emissivities $j(S_2)$ and $j(R_2)$ were derived from the five-level-atom solution for S^+ and O^+ . The energy levels and the

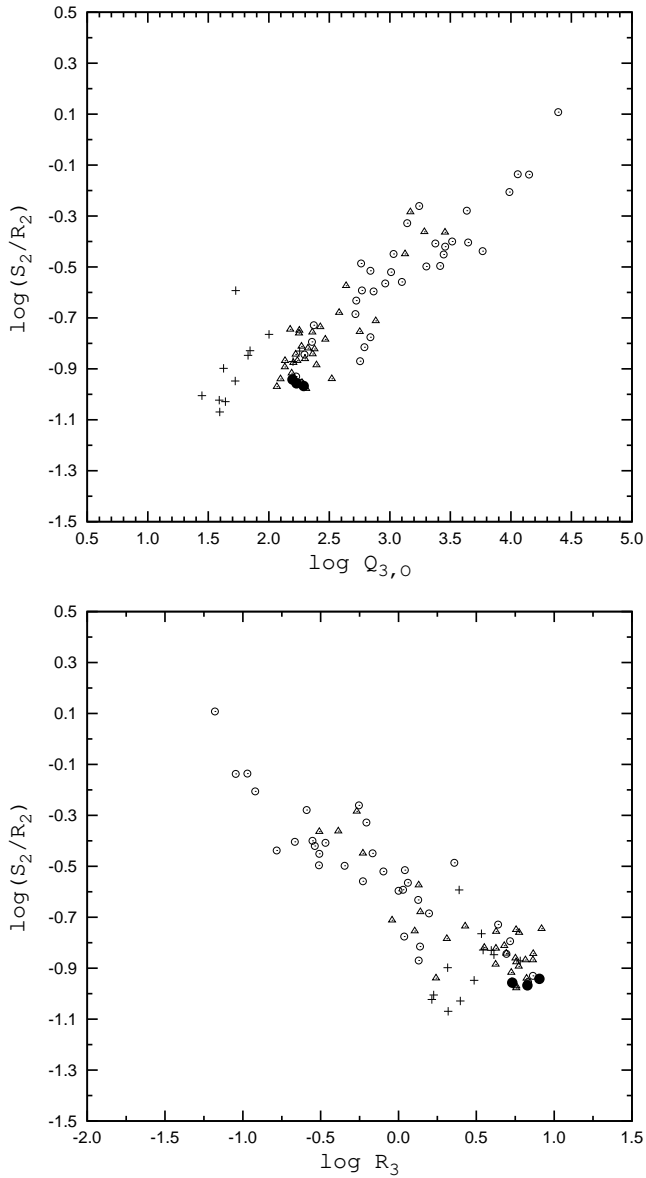


Figure 18. The S_2/R_2 line ratio as a function of $Q_{3,O}$ (*top panel*) and R_3 line flux (*bottom panel*). The open circles are high-metallicity H II regions with $\Delta t_{2,N} < 0.1$, the filled circles are those with $\Delta t_{2,N} > 0.1$, the open triangles are objects without $t_{2,N}$ measurements. The plus signs show the low-metallicity H II regions in the dwarf irregular galaxy DDO 68.

Einstein coefficients for spontaneous transitions for five low-lying levels for S^+ were taken from Irimia & Froese Fisher (2003), the effective collision strengths for the electron impact were taken from Keenan et al. (1996). The atomic data for O^+ were discussed above. Fig. 17 shows a clear correlation between S_2/R_2 and t_2 .

Since there is a one-to-one correspondence between the t_2 and t_3 electron temperatures for high-metallicity H II regions, one might expect that there is also a correlation between S_2/R_2 and t_3 . The use of the S_2/R_2 vs. t_3 instead of the S_2/R_2 vs. t_2 diagram has the advantage that the direct measurements of $t_{3,O}$ in high- R_3 H II regions are available in greater numbers than are direct measurements of $t_{2,O}$ and/or $t_{2,N}$. The top panel of Fig. 18 shows the $Q_{3,O}$

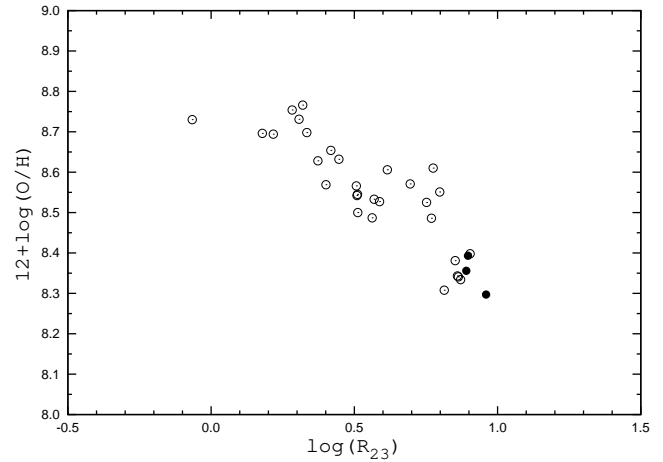


Figure 19. $R_{23} - O/H$ diagram. The open circles are H II regions with $\Delta t_{2,N} < 0.1$ or with $\Delta t_{2,O} < 0.1$, the filled circles are those with $\Delta t_{2,N} > 0.1$.

vs. S_2/R_2 diagram. The open circles are H II regions with $\Delta t_{2,N} < 0.1$, the filled circles are those with $\Delta t_{2,N} > 0.1$, the open triangles are objects where $t_{2,N}$ is not measured. The low-metallicity ($12+\log(O/H) \sim 7.2$) H II regions in the dwarf galaxy DDO 68 (Pustilnik, Kniazev & Pramskij 2005) are shown for comparison (plus signs). Fig. 18 (the top panel) shows a clear correlation between S_2/R_2 and $Q_{3,O}$; the S_2/R_2 line ratio decreases with decreasing of $Q_{3,O}$. In fact, the S_2/R_2 value can be used as an alternative indicator of the t_3 , although the scatter in the $Q_{3,O}$ vs. S_2/R_2 relation is large. Fig. 18 (top panel) shows that the H II regions with large deviations follow the general trend, although they are located near the end of the sequence.

The bottom panel of Fig. 18 shows a R_3 vs. S_2/R_2 diagram. The H II regions with $\log R_3 > 0.5$ show a shift relative to the general trend obtained from the H II regions with $\log R_3 < 0.5$. There are two possible causes for this shift. Either the high- R_3 and the low- R_3 H II regions do not belong to the same sequence (the upper branch), or the line fluxes of low-ionisation ions (N^+ , O^+ , S^+) are distorted in H II regions with strong R_3 line fluxes.

Our sample only contains H II regions with $12+\log(O/H) > 8.2$. This selection criterion comes from the following consideration. It is well known that the relation between the oxygen abundance and the strong oxygen-line intensities is double valued with two distinct sequences, traditionally known as the upper and the lower branches of the $R_{23} - O/H$ diagram. The transition zone between the upper and the lower branches is sometimes also taken into consideration (Pilyugin & Thuan 2005). We adopt $12+\log(O/H) = 8.2$ as the boundary between the upper branch and the transition zone. This division is somewhat arbitrary, however. Fig. 19 shows the $R_{23} - O/H$ diagram for the H II regions with measured $t_{2,N}$ or $t_{2,O}$ temperature. The question is, if one should adopt a higher oxygen abundance (e.g., $12+\log(O/H) = 8.4$) as the boundary between the upper branch and the transition zone? We believe that is probably not the way to solve the problem. It should be noted that both H II regions with small deviations and H II regions with large deviations follow the ff relation for $Q_{3,O}$ rather well. Furthermore,

Fig. 19 shows that the area occupied by the H II regions with large deviations is also populated by the H II regions with small deviations. Finally, some high-metallicity galactic H II regions also show large deviations. It is possible that a criterion other than a specific metallicity should be used to divide the H II regions into sequences (branches).

The deviations suggest that the $Q_{2,N}$ values are shifted in H II regions with strong R_3 line fluxes (high excitation parameter P). It has been suggested that the low-lying metastable levels in some ions are excited not only by the electron collisions, but may also be significantly populated by recombination processes (Rubin 1986; Liu et al. 2000). Since recombination-excited emission of [O II] in the auroral $\lambda 7325$, and [N II] in the auroral $\lambda 5755$ radiation will occur in the O^{++} zone, the effect on the collision-excited lines will depend on the R_3 line flux. As a result, one may expect a significant shift of the $Q_{2,N}$ and $Q_{2,O}$ values for H II regions with strong R_3 line fluxes. Our results are generally in agreement with this picture. However, other mechanisms causing a shift of this kind of the $Q_{2,N}$ value cannot be excluded.

6 CONCLUSIONS

The electron temperatures of high-metallicity ($12 + \log(O/H) > 8.2$) H II regions have been studied. Empirical ff relations which express the nebular-to-auroral lines ratios ($Q_{3,O}$, $Q_{2,O}$, and $Q_{2,N}$) in terms of the nebular R_3 and R_2 line fluxes in spectra of H II regions have been derived. The ff relations for $Q_{2,O}$ and $Q_{2,N}$ only reproduce the observational data in spectra of H II regions with weak nebular R_3 line fluxes ($\log R_3 \lesssim 0.5$). The ff relation for $Q_{3,O}$, on the other hand, reproduces the observational data over the whole range of nebular R_3 line fluxes.

The $t_2 - t_3$ diagram has also been considered. We found that there is a one-to-one correspondence between the t_2 and t_3 electron temperatures, within the uncertainties of these electron temperatures, for H II regions with weak nebular R_3 line fluxes. The derived $t_{2,N} - t_{3,O}$ relation for these H II regions is very similar to the commonly used $t_2 - t_3$ relation after Campbell, Terlevich & Melnick (1986). The H II regions with strong nebular R_3 line fluxes do not follow this relation, however. Thus, as a result, the one-to-one correspondence between the electron temperatures $t_{2,N}$ and $t_{3,O}$ disappears if H II regions with both weak and strong R_3 line fluxes are included.

There is a discrepancy between $t_{2,N}$ and $t_{2,O}$ temperatures. The $t_{2,N}$ temperatures are systematically lower than the $t_{2,O}$ temperatures. The difference is small at low electron temperatures and increases with the electron temperature to about 10% at $t = 1$. The uncertainties in the atomic data (Einstein coefficients for spontaneous transitions and effective cross sections for electron impact) may be the cause of this discrepancy.

ACKNOWLEDGMENTS

We thank the referee, F.P. Keenan, for constructive criticism and useful comments that helped to improve the paper. We also thank N. Bergvall for useful discussions on line-blending effects.

REFERENCES

- Aggarwal K.M., Keenan F.P. 1999, ApJS, 123, 31
 Baldwin J.A., Verner E.M., Verner D.A., Ferland G.J., Martin P.G., Korista K.T., Rubin R.H., 2000, ApJS, 129, 229
 Bresolin F., Garnett D.R., Kennicutt R.C., 2004, ApJ, 615, 228
 Bresolin F., Schaerer D., Conzález Delgado R.M., Stasińska, G. 2005, A&A, 441, 981
 Bresolin F., 2007, ApJ, 656, 186
 Bresolin F., Gieren W., Kudritzki R.-P., Pietrzyński G., Urbaneja M.A., 2009, ApJ, accepted (astro-ph/0905.2791)
 Campbell A., Terlevich R., Melnick J., 1986, MNRAS, 223, 811
 Crockett N.R., Garnett D.R., Massey P., Jacoby G. 2006, ApJ, 637, 741
 Deharveng L., Peña M., Caplan J., Costero R., 2000, MNRAS, 311, 329
 Edlén B. 1985, Phys. Scripta, 31, 345
 Esteban C., Peimbert M., Torres-Peimbert S., García-Rojas J., 1999a, Rev.Mex. A&A, 35, 65
 Esteban C., Peimbert M., Torres-Peimbert S., García-Rojas J., Rodríguez M., 1999b, ApJS, 120, 113
 Esteban C., Peimbert M., García-Rojas J., Ruiz M.T., Peimbert A., Rodríguez M., 2004, MNRAS, 355, 229
 Esteban C., Peimbert M., García-Rojas J., Peimbert A., Mesa-Delgado A., 2009, ApJ, accepted (astro-ph/0905.2532)
 Froese Fischer C., Tachiev G. 2004, ADNDT, 87, 1
 Galavís M.E., Mendoza C., Zeppen C.J. 1997, A&AS, 123, 159
 García-Rojas J., Esteban C., Peimbert M., Rodríguez M., Ruiz M.T., Peimbert A., 2004, ApJS, 153, 501
 García-Rojas J., Esteban C., Peimbert A., Peimbert M., Rodríguez M., Ruiz M.T., 2005, MNRAS, 362, 301
 García-Rojas J., Esteban C., Peimbert M., Costado M.T., Rodríguez M., Peimbert M., Ruiz M.T., 2006, MNRAS, 368, 253
 García-Rojas J., Esteban C., Peimbert A., Rodríguez M., Peimbert M., Ruiz M.T., 2007, Rev.Mex.A&A, 43, 3
 Garnett D.R., 1992, AJ, 103, 1330
 Garnett D., Kennicutt R.C., Bresolin F. 2004, ApJ, 607, L21
 Guseva N.G., Izotov Y.I., Thuan T.X. 2000, ApJ, 531, 776
 Hudson C.E., Bell K.L. 2004, MNRAS, 348, 1275
 Hudson C.E., Bell K.L. 2005, A&A, 430, 725
 Irimia A., Froese Fisher C., 2003, <http://hf8.vuse.vanderbilt.edu>
 Izotov Y.I., Thuan T.X. 2004, ApJ, 602, 200
 Izotov Y.I., Thuan T.X., Lipovetsky V.A., 1997, ApJS, 108, 1
 Keenan F.P., Aller L.H., Bell K.L., Hyung S., McKenna F.C., Ramsbottom C.A., 1996, MNRAS 281, 1073
 Kennicutt R.C., Bresolin F., Garnett D. 2003, ApJ, 591, 801
 Lee H., McCall M.L., Kingsburgh R.L., Ross R., Stevenson C. 2003, AJ, 125, 146
 Lee H., Skillman E.D. 2004, ApJ, 614, 698
 Lee H., Salzer J.J., Melbourne J. 2004, ApJ, 616, 752
 Liu X.-W., Storey P.J., Barlow M.J., Danziger I.J., Cohen M., & Bryce M., 2000, MNRAS, 312, 585

- Lodders K. 2003, ApJ, 591, 1220
 Luridiana V., Esteban C., Peimbert M., Peimbert A. 2002, RevMexAA, 38, 97
 Oey M.S., Shields J.C., 2000, ApJ, 539, 687
 Pagel, B.E.J., Simonson, E.A., Terlevich, R.J., & Edmunds, M.G. 1992, MNRAS, 255, 325
 Peimbert A., 2003, ApJ, 584, 735
 Pilyugin L.S., 2000, A&A, 362, 325
 Pilyugin L.S., 2001, A&A, 369, 594
 Pilyugin L.S., 2003, A&A, 399, 1003
 Pilyugin L.S., 2005, A&A, 436, 1L
 Pilyugin L.S. 2007, MNRAS, 375, 685
 Pilyugin L.S. 2009, Kinematika i fizika nebesnyh tel (in russian), accepted
 Pilyugin L.S., Thuan T.X., Vílchez J.M., 2006a, MNRAS, 367, 1139
 Pilyugin L.S., Thuan T.X., 2005, ApJ, 631, 231
 Pilyugin L.S., Thuan T.X., 2007, ApJ, 669, 290
 Pilyugin L.S., Vílchez J.M., Thuan T.X., 2006b, MNRAS, 370, 1928
 Pradhan A.K., Montenegro M., Nahar S.N., Eissner W. 2006, MNRAS, 366, L6
 Pustilnik S.A., Kniazev A.Y., Pramskij A.G. 2005, A&A, 443, 91
 Rubin R.H., 1986, ApJ, 309, 334
 Thuan T.X., Izotov Y.I. 2005, ApJS, 161, 240
 Tayal S.S., 2007, ApJS, 171, 331
 Tsamis Y.G., Barlow M.J., Liu X.-W., Danziger I.J., Storey P.J., 2003, MNRAS, 338, 687
 Vermeij R., Damour F., van der Hulst, J.M., Baluteau J.-P., 2002, A&A, 390, 649
 Vílchez J.M., Iglesias-Páramo J. 2003, ApJS, 145, 225
 Wenåker I. 1990, Phys. Scripta, 42, 667
 Zaritsky D., Kennicutt R.C., Huchra J.P. 1994, ApJ, 420, 87
- C06 – Crockett et al (2006),
 B07 – Bresolin (2007).
 The measured [O II] λ 3727+ λ 3729, [O III] λ 4363, [O III] λ 4959+ λ 5007, [N II] λ 5755, [N II] λ 6548+ λ 6584, [S II] λ 6717+ λ 6731, [O II] λ 7320+ λ 7330 line intensities are listed in columns from 3 to 9 respectively. The line intensities are given on a scale where $H\beta = 1$.

APPENDIX A: A SAMPLE OF THE CALIBRATION H II REGIONS. ONLINE MATERIAL

Table A1 contains the line intensities measured in the spectra of the calibration H II regions. The first column gives the object name (which is typically the name of the parent galaxy and the H II region identifier). The second column provides the data-source reference. The following abbreviations for the references are used:

- G00 – Guseva, Izotov & Thuan (2000),
 L02 – Luridiana et al. (2002),
 V02 – Vermeij et al. (2002),
 K03 – Kennicutt, Bresolin & Garnett (2003),
 L03 – Lee et al. (2003),
 T03 – Tsamis et al. (2003),
 P03 – Peimbert (2003),
 V03 – Vílchez & Iglesias-Páramo (2003),
 B04 – Bresolin et al. (2004),
 I04 – Izotov & Thuan (2004),
 G04 – Garnett, Kennicutt & Bresolin (2004),
 L04a – Lee, Salzer & Melbourne (2004),
 L04b – Lee & Skillman (2004),
 B05 – Bresolin et al. (2005),
 T05 – Thuan & Izotov (2005),

Table A1. Line intensities of the sample of calibration H II regions. The line intensities are given on a scale where $H\beta = 1$.

Object name identifier	Reference	[O II] $\lambda 3727$	[O III] $\lambda 4363$	[O III] $\lambda 4959+5007$	[N II] $\lambda 5755$	[N II] $\lambda 6548+6584$	[S II] $\lambda 6717+6731$	[O II] $\lambda 7320+7330$
Mrk 1329	G00	1.152	0.0460	7.308	0.00000	0.099	0.156	0.0000
M101 N5461	L02	1.914	0.0119	4.361	0.00400	0.566	0.357	0.0415
SMC N160A1	V02	1.655	0.0000	5.635	0.00000	0.249	0.228	0.0460
LMC N4A	V02	1.522	0.0000	5.720	0.00000	0.177	0.160	0.0400
M101 H67	K03	2.440	0.0350	4.560	0.00000	0.217	0.263	0.0540
M101 H70	K03	3.110	0.0250	3.560	0.00000	0.315	0.472	0.0000
M101 H128	K03	1.450	0.0170	5.213	0.00300	0.277	0.233	0.0410
M101 H149	K03	2.120	0.0180	4.240	0.00000	0.479	0.372	0.0560
M101 H336	K03	1.780	0.0000	0.308	0.00500	1.278	0.568	0.0140
M101 H409	K03	2.180	0.0230	4.931	0.00400	0.364	0.312	0.0470
M101 H1013	K03	1.880	0.0000	1.373	0.00500	0.861	0.288	0.0260
M101 H1105	K03	1.850	0.0140	4.210	0.00000	0.445	0.241	0.0360
M101 H1159	K03	1.980	0.0190	4.227	0.00000	0.315	0.298	0.0480
M101 H1170	K03	3.080	0.0160	2.680	0.00000	0.587	0.567	0.0000
M101 H1176	K03	1.600	0.0240	4.920	0.00000	0.283	0.230	0.0300
IC10 # 1	L03	1.980	0.0237	4.834	0.00000	0.000	0.000	0.0000
IC10 # 2	L03	1.750	0.0220	4.929	0.00000	0.000	0.000	0.0000
LMC 30 Dor	T03	1.056	0.0335	6.730	0.00206	0.120	0.114	0.0377
LMC 30 Dor	P03	1.235	0.0321	6.788	0.00187	0.152	0.137	0.0373
VCC1699	V03	1.260	0.0410	7.350	0.00000	0.104	0.181	0.0000
VCC144	V03	2.541	0.0240	4.782	0.00000	0.274	0.392	0.0000
M51 CCM10	B04	1.260	0.0000	0.165	0.00500	1.490	0.460	0.0000
M51 CCM53	B04	1.290	0.0000	0.451	0.00540	1.600	0.410	0.0000
M51 CCM54	B04	1.150	0.0000	0.557	0.00650	1.620	0.630	0.0000
M51 CCM55	B04	0.780	0.0000	0.257	0.00430	1.550	0.410	0.0000
M51 CCM57	B04	1.140	0.0000	0.216	0.00680	1.640	0.450	0.0000
M51 CCM57A	B04	1.040	0.0000	2.286	0.00480	0.930	0.340	0.0000
M51 CCM71A	B04	1.470	0.0000	0.622	0.00790	1.550	0.690	0.0000
M51 CCM72	B04	0.630	0.0000	0.090	0.00280	1.330	0.460	0.0000
M51 CCM84A	B04	1.250	0.0000	1.147	0.00920	1.930	0.340	0.0000
M51 P203	B04	0.320	0.0000	0.066	0.00150	1.050	0.410	0.0000
HS0111+2115	I04	3.207	0.0389	5.928	0.00000	0.259	0.410	0.0000
UM396	I04	1.117	0.0588	8.290	0.00000	0.108	0.201	0.0000
Mrk 35	I04	2.509	0.0273	5.380	0.00370	0.265	0.277	0.0468
Mrk 1315	I04	1.085	0.0522	8.039	0.00130	0.078	0.124	0.0000
Mrk 1329	I04	1.242	0.0443	7.309	0.00130	0.094	0.146	0.0208
M51 CCM72	I04	0.670	0.0000	0.107	0.00200	1.380	0.490	0.0000
KISSR 87	L04a	1.895	0.0280	5.958	0.00000	0.302	0.329	0.0000
KISSR 286	L04a	2.053	0.0370	5.683	0.00000	0.204	0.366	0.0400
NGC1705 A3	L04b	2.540	0.0410	5.720	0.00000	0.124	0.338	0.0000
NGC1705 B3	L04b	2.740	0.0560	6.530	0.00000	0.131	0.371	0.0000
NGC1705 B4	L04b	3.120	0.0480	6.650	0.00000	0.092	0.358	0.0000
NGC1705 B6	L04b	4.360	0.0570	5.720	0.00000	0.197	0.467	0.0000
NGC1705 C6	L04b	3.018	0.0330	5.303	0.00000	0.083	0.365	0.0000
NGC1232 # 2	B05	3.910	0.0000	1.740	0.00000	0.640	0.450	0.0840
NGC1232 # 4	B05	2.070	0.0000	5.360	0.00000	0.290	0.230	0.0400
NGC1232 # 5	B05	2.530	0.0000	1.340	0.00540	1.110	0.590	0.0340
NGC1232 # 6	B05	2.110	0.0000	0.680	0.00660	1.200	0.750	0.0320
NGC1232 # 7	B05	1.630	0.0000	0.290	0.00390	1.560	0.620	0.0140
NGC1232 # 10	B05	1.340	0.0000	0.310	0.00000	1.230	0.580	0.0120
NGC1232 # 14	B05	3.050	0.0000	1.070	0.00840	1.270	0.780	0.0540
NGC1232 # 15	B05	4.580	0.0000	1.380	0.00000	0.760	0.960	0.0910
NGC1365 # 3	B05	2.420	0.0000	0.910	0.00000	1.130	0.470	0.0240
NGC1365 # 5	B05	1.690	0.0000	0.340	0.00450	1.350	0.660	0.0160
NGC1365 # 8	B05	1.720	0.0000	0.800	0.00660	1.150	0.520	0.0200
NGC1365 # 12	B05	1.750	0.0000	0.410	0.00000	1.380	0.760	0.0160
NGC1365 # 15	B05	2.210	0.0000	1.000	0.00920	1.690	0.560	0.0310
NGC1365 # 16	B05	2.440	0.0000	1.270	0.00000	0.910	0.430	0.0400
NGC1365 # 17	B05	3.600	0.0000	1.350	0.00000	1.150	0.960	0.0560

Table A1. Continued

Object name	Reference	[O II] $\lambda 3727$	[O III] $\lambda 4363$	[O III] $\lambda 4959+5007$	[N II] $\lambda 5755$	[N II] $\lambda 6548+6584$	[S II] $\lambda 6717+6731$	[O II] $\lambda 7320+7330$
NGC2997 # 4	B05	3.830	0.0000	2.040	0.00000	0.800	0.630	0.0660
NGC2997 # 5	B05	2.130	0.0000	1.100	0.00460	1.160	0.650	0.0340
NGC2997 # 6	B05	2.150	0.0000	1.090	0.00580	1.130	0.360	0.0320
NGC2997 # 7	B05	2.030	0.0000	0.590	0.00640	1.340	0.560	0.0250
NGC2997 # 11	B05	1.710	0.0000	0.540	0.00000	1.410	0.890	0.0270
NGC2997 # 14	B05	1.770	0.0000	0.590	0.00000	1.290	0.630	0.0240
NGC5236 # 3	B05	2.080	0.0000	1.570	0.00740	1.300	0.430	0.0290
NGC5236 # 6	B05	1.230	0.0000	0.280	0.00810	1.650	0.490	0.0120
NGC5236 # 14	B05	0.740	0.0000	0.120	0.00420	1.460	0.460	0.0060
NGC5236 # 16	B05	1.440	0.0000	0.310	0.00600	1.790	0.510	0.0000
Mrk 35 # 1	T05	1.874	0.0265	5.408	0.00000	0.000	0.000	0.0000
M33 BCLMP090	C06	1.980	0.0410	8.760	0.00000	0.000	0.000	0.0000
M33 BCLMP691	C06	1.680	0.0220	4.560	0.00000	0.000	0.000	0.0000
M33 BCLMP706	C06	2.790	0.0120	2.910	0.00000	0.000	0.000	0.0000
M33 BCLMP290a	C06	2.230	0.0110	2.490	0.00000	0.000	0.000	0.0000
M33 MA 1	C06	1.140	0.0430	6.980	0.00000	0.000	0.000	0.0000
M101 H1013	B07	2.210	0.0024	1.350	0.00590	0.950	0.298	0.0240